Contents lists available at ScienceDirect

EBioMedicine

EBioMedicine
Published by THE LANCET

A new gold(I) complex-Au(PPh₃)PT is a deubiquitinase inhibitor and inhibits tumor growth

Xiaofen Li [a,b,1], Qingtian Huang [b,1], Huidan Long [b,1], Peiquan Zhang [b], Huabo Su [a,b,c], Jinbao Liu [a,b,*]

[a] Affiliated Cancer Hospital & Institute of Guangzhou Medical University, Guangzhou, Guangdong 510095, China
[b] Protein Modification and Degradation Lab, State Key Lab of Respiratory Disease, Guangzhou Medical University, Guangdong, China
[c] Vascular Biology Center, Medical College of Georgia, Augusta University, Augusta, GA, USA

ARTICLE INFO

ABSTRACT

Background: Ubiquitin-proteasome system (UPS) is integral to cell survival by maintaining protein homeostasis, and its dysfunction has been linked to cancer and several other human diseases. Through counteracting ubiquitination, deubiquitinases (DUBs) can either positively or negatively regulate UPS function, thereby representing attractive targets of cancer therapies. Previous studies have shown that metal complexes can inhibit tumor growth through targeting the UPS; however, novel metal complexes with higher specificity for cancer therapy are still lacking.
Methods: We synthesized a new gold(I) complex, Au(PPh₃)PT. The inhibitory activity of Au(PPh₃)PT on the UPS and the growth of multiple cancer cell types were tested *in vitro*, *ex vivo*, and *in vivo*. Furthermore, we compared the efficacy of Au(PPh₃)PT with other metal compounds in inhibition of UPS function and tumor growth.
Findings: Here we report that (i) a new gold(I) complex-pyrithione, *i.e.*, Au(PPh₃)PT, induced apoptosis in two lung cancer cell lines A549 and NCI-H1299; (ii) Au(PPh₃)PT severely impaired UPS proteolytic function; (iii) Au(PPh₃)PT selectively inhibited 19S proteasome-associated DUBs (UCHL5 and USP14) and other non-proteasomal DUBs with minimal effects on the function of 20S proteasome; (iv) Au(PPh₃)PT induced apoptosis in cancer cells from acute myeloid leukemia patients; (v) Au(PPh₃)PT effectively suppressed the growth of lung adenocarcinoma xenografts in nude mice; and (vi) Au (PPh₃)PT elicited less cytotoxicity in normal cells than several other metal compounds.
Interpretation: Together, this study discovers a new gold(I) complex to be an effective inhibitor of the DUBs and a potential anti-cancer drug.

1. Introduction

The ubiquitin-proteasome system (UPS) is the primary degradation machinery of intracellular proteins and regulates numerous cellular and pathophysiological events [1]. Not surprisingly, its dysfunction has been linked to the pathogenesis of a wide array of human diseases, including neuronal degenerative disorders, cardiovascular diseases, viral infection, and tumorigenesis [2–5]. A variety of cancer cells such as colon cancer, prostate cancers, and leukemia possess a hyperactive proteasome system, suggesting that cancer cells may rely more heavily on the UPS to defend against cellular stresses than non-cancer cells. Indeed, accumulating evidence has demonstrated the effectiveness of targeting UPS for cancer treatment [6,7]. The 26S proteasome is assembled by the 20S core complex and the 19S regulatory complex. Bortezomib (Velcade, Vel) is the first compound developed to specifically inactivate the enzymatic activity of the 20S proteasome and subsequently approved by U.S. FDA to treat multiple myeloma in 2003 [8]. Since then, Vel-based therapy has greatly benefited many cancer patients and improved the overall survival rate of these patients. However, clinical data revealed that Vel-based therapy often associates with relapses and toxicities and has minimal effects on solid tumors [9,10]. Therefore, there is an urgent need for the discovery of new

Research in context

Evidence before this study

Deubiquitinases (DUBs), especially the 19S proteasome-associated deubiquitinases are promising therapeutic targets in cancer treatment. While inhibitors of DUBs were recently reported and shown experimentally to exhibit anticancer effects, the suitability of these inhibitors for clinical use remains to be tested.

Added value of this study

In this study, we identify a novel metal-containing compound, Au(PPh₃)PT, that inhibits the activity of 19S proteasome-associated and other deubiquitinases. Furthermore, Au(PPh₃)PT induces apoptosis in lung cancer cell lines *in vitro*, are selectively toxic to bone marrow cells from acute myeloid leukemia patients *ex vivo*, and has a high potency of inhibition of the growth of lung adenocarcinoma xenografts *in vivo*.

Implications of all the available evidence

This study discovers a new gold(I) complex to be a novel and potent inhibitor of deubiquitinases with potential utility in cancer treatment.

potent and selective proteasome inhibitors with little to no toxicity for cancer treatment.

Deubiquitinases (DUBs) are a class of enzymes that deconjugate ubiquitin from ubiquitinated proteins. DUBs regulate many cellular processes, including cell cycle [11], protein proteolysis [12], transcriptional gene expression [13], and DNA damage response [14,15]. Mutations in several DUBs are implicated in human diseases such as cancer and neurological disorders [16–18]. The human genome encodes 98 putative DUBs [19]. Among them, three DUBs are associated with the 19S regulatory particles: POH1/RPN11, USP14/Ubp6, and UCHL5/Uch37. USP14/Ubp6 and UCHL5/Uch37 are cysteine proteases and belong to the ubiquitin specific protease (USP) and ubiquitin C-terminal hydrolases (UCH) families, respectively. POH1/RPN11 is a Zn^{2+}-dependent protease of the JAB1/MPN/Mov34 (JAMM) family and an intrinsic subunit of the lid of the 19S proteasome [20]. The physiological roles of the 19S proteasome-associated DUBs are not well understood [21–23]. Many of DUBs have been identified as oncogenes or tumor suppressors, likely functioning to regulate the stability of key proteins involved in tumorigenesis [24]. And increasing evidence suggests that DUBs are attractive therapeutic targets for cancer [25]. Unlike 20S proteasome inhibitors that block protein degradation with limited substrate specificity, most of the reported DUB inhibitors selectively target one or several DUBs and thus only regulate the expression of a subset of cellular proteins. Interference with the DUBs, especially the 19S proteasome-associated DUBs, could be more effective in limiting the growth of cancer cells and more tolerable to normal cells [25,26].

We and others have previously demonstrated that metal-containing compounds inhibit the proteasome peptidase activities and induce cytotoxicity in cancer cells [27–31]. Pyrithione (PT) possesses excellent metal chelating properties. The nickel and zinc complexes of pyrithione (NiPT and ZnPT), for example, has significant anticancer effects through inhibiting the 19S proteasome-associated DUBs [30,31]. Moreover, we have recently show that copper pyrithione (CuPT) has potent inhibitory effects on UPS function through inactivation of both the 19S and 20S proteasome and exhibits strong cytotoxic effects in cancer cells [27]. In this current work, we report that a new gold(I) complex, Au(PPh₃) PT, inhibits the activity of 19S proteasome-associated and other DUBs but has little impact on the proteolytic activities of the 20S proteasome,

leading to a rapid buildup of ubiquitinated proteins. While induces less cytotoxicity in normal cells, Au(PPh₃)PT is cytotoxic to lung cancer cells and pathogenic bone marrow cells isolated from AML patients, and effectively represses the growth of lung adenocarcinoma xenografts in nude mice. Hence, Au(PPh₃)PT could be a highly promising anticancer compound.

2. Materials and methods

2.1. Materials

Au(PPh₃)PT,NiPT, and CuPT were synthesized in our laboratory and stored as a 2 mM stock solution in dimethyl sulfoxide (DMSO) at −20 °C. Velcade (bortezomib, PS341) was purchased from BD Biosciences (San Jose, CA, USA). N-ethylmaleimide (NEM), Cisplatin (CDDP), *N*-acetyl-Lcysteine (NAC), and *tert*-Butylhydroquinone (tBHQ) were purchased from Sigma-Aldrich (St. Louis, MO, USA). Pan caspase Inhibitor *Z*-VAD-FMK was purchased from EnzoLife Sciences International (Inc, Plymouth Meeting, PA, USA). b-AP15, Suc-Leu-Leu-Val-Tyr-AMC (Suc-LLVY-AMC), Z-Leu-Leu-Glu-AMC (Z-LLE-AMC), Boc-Leu-Arg-Arg-AMC (Boc-LRR-AMC), 20S and 26S human proteasome preparations, HA-Ubiquitin-Vinyl Sulfone (HA-Ub-*VS*), and K48-linked tetra-ubiquitin Ubiquitin-AMC (U550) were purchased from Boston Biochem (Cambridge, MA, USA). Antibodies used in this study were from the following sources: anti-GFP (B-2) was from Santa Cruz Biotechnology (Santa Cruz, CA, USA); anti-caspase 3 (8G10), anti-caspase 8 (1C12), anti-caspase 9 (C9), anti-cleaved caspase-8 (18C8), anti-PARP, anti-USP7, anti-USP10, anti-USP15, anti-USP25, anti-p-ATM, anti-p-CHK1, anti-p-CHK2, and anti-γ-H2AX were purchased from Cell Signaling Technology (Beverly, MA, USA); anti-K48-linkage specific polyubiquitin (D9D5), anti-GAPDH, anti-HA-tag, anti-cleaved caspase-3, and anti-cleaved caspase-9 were from Bioworld Technology (St. Louis Park, MN, USA); anti-UCHL5/Uch37 (Epitomics) and anti-USP14 (C-term) were from ABGENT (San Diego, CA, USA); anti-Ki67 was from Servicebio Technology CO., LTD (Wuhan, China). Annexin V- fluoroisothiocyanate (FITC) / propidium iodide (PI) apoptosis detection kit and reactive oxygen species assay kit were purchased from Keygen Company (Nanjing, China). Enhanced chemiluminescence (ECL) reagents were purchased from Santa Cruz Biotechnology (Santa Cruz, CA, USA).

2.2. Syntheses and structure determination of Au(PPh₃)PT

Au(PPh₃)PT was synthesized by our laboratory. Au(PPh₃)PT (49 mg, 0.1 mmol) was dissolved in 20 ml of dichloromethane (CH_2Cl_2) followed by the addition of 2-mercaptopyridine-1-oxide sodium (Nampo; 20 mg, 0.1 mmol). The reaction mixture was stirred for six hours before subsequent filtration. The resulting filtrate was allowed to evaporate at ambient atmosphere for five days. Block-shaped light yellow crystals of complex Au(PPh₃)PT were collected, washed by ethanol, and air dried.

Single crystal of complex Au(PPh₃)PT (size: 0.20 mm × 0.20 mm × 0.15 mm) was subjected to single crystal X-ray analysis. The diffraction data was collected on a Rigaku Mercury CCD and the data were collected using a graphite monochromator Mo Kα radiation ($\lambda = 0.071073$ nm) at 293(2) K. A total of 23,432 reflection was collected with 7439 unique one (Rint = 0.2396 0.2376) for complex Au(PPh₃)PT. Lorentz factor, polarization, air absorption and absorption due to variations in the path length through the detector faceplate were applied to correct the data sets. Absorption correction based on Multi-scan method was also applied. The structure of Au(PPh₃)PT was solved using direct methods (SHELXTL) and refined by full-matrix least-square techniques with atomic coordinates and anisotropic temperature factors for all non-hydrogen atoms. The hydrogen atoms attached to C and O atoms were added according to theoretical models, and their positions and thermal parameters were fixed during the structure refinement. For complex Au(PPh₃)PT, the final R1 = 0.1154 and wR2 = 0.2670, S = 1.012, $(\Delta\rho)_{max}$

$= 6.04$ and $(\triangle\rho)_{min} = -1.67$ e·Å^{-3} for 4151 observed reflections ($I > 2\sigma(I)$) with 253 parameters.

2.3. Cell lines and cell viability assay

Human lung cancer cell lines A549 and NCI-H1299, and human epithelial lung cell line BEAS-2B were obtained from American Type Culture Collection (Manassas, VA, USA). A549 and NCI-H1299 cell lines were cultured in RPMI 1640, while BEAS-2B cell line was cultured in F12. Both of these media were supplemented with 10% FBS, 100 units/ml of penicillin, and 100 μg/ml of streptomycin. Cell cultures were maintained at 37 °C and 5% CO$_2$. The CellTiter 96® AQueous One Solution Cell Proliferation Assay (MTS) (Promega, Shanghai, China) was performed to test cell viability as previously reported [32]. Briefly, A549, NCI-H1299, and BEAS-2B cells were plated onto 96-well plates at a total of 10,000 cells/well, then treated with either vehicle or Au(PPh$_3$)PT, NiPT, CuPT for 24, 48, or 72 h before performing the MTS assay. MTS assay reagent (20 μl) was added to each well of the 96-well plate three hours before the termination of the experiments. The absorbance at 490 nm was detected using a plate reader (Varioskan Flash 3001, Thermo, Waltham, MA, USA). The concentrations of each compound that induce 50% inhibition of cell growth (IC$_{50}$) values were derived.

2.4. Cell death assay

Apoptotic rates were assessed by flow cytometry using Annexin V-fluoroisothiocyanate (FITC)/propidium iodide (PI) (Keygen, Nanjing, China) double staining [32]. After treatment with Au(PPh$_3$)PT at various concentrations for 24 h, cells were collected and washed with binding buffer, then incubated with Annexin V-FITC followed by the addition of PI prior to analysis. In addition, cells were submitted to Annexin V/PI staining *in situ*, then imaged with an inverted fluorescence microscope equipped with a digital camera (Axio Obsever Z1, Zeiss, Germany).

2.5. Western blot analysis

After treatment, the cells were lysed in RIPA buffer (1 × PBS, 1% NP-40, 0.5% sodium deoxycholate, 0.1% SDS) supplemented with 10 mM β-glycerophosphate, 1 mM sodium orthovanadate, 10 mM NaF, 1 mM phenylmethylsulfonyl fluoride (PMSF), and 1× Roche Complete Mini Protease Inhibitor Cocktail (Roche, Indianapolis, IN). SDS-PAGE, transferring, and immunodetection were performed as previously described [33]. In brief, an equal amount of total protein was resolved by SDS-PAGE and electro-transferred onto polyvinylidene difluoride (PVDF) membranes. After blocking with 5% milk, primary antibodies and appropriate horseradish peroxidase (HRP)-conjugated secondary antibodies were used to detect the designated proteins. ECL detection reagents (Santa Cruz, CA, USA) were used for detection, and bands were revealed by autoradiography (Kodak, Japan).

2.6. Sample collection and cell culture

The use of human samples is approved by the Institution with the permission of the patients and volunteers. Seven patients with AML and six healthy volunteers were recruited in this preclinical study. Bone marrow and blood samples of patients with AML were obtained from the Department of Hematology (Second Affiliated Hospital, Guangzhou Medical University). Peripheral blood samples of normal control individuals were obtained from Guangzhou Blood Center. Ficoll-Paque (Pharmacia, Uppsala, Sweden) was used to isolate mononuclear cells from either peripheral blood or bone marrow samples by density gradient. The mononuclear cells were cultured in RPMI 1640 culture medium with 15% FBS as described previously [31].

2.7. Peptidase activity assay

Briefly, purified human 20S proteasome was incubated with 2.5, 5, 10, 20 μM Au(PPh$_3$)PT or 0.1 μM Velcade for 60 min at 37 °C before the addition of fluorogenic substrates. The 20S proteasome activity was measured by the release of hydrolyzed AMC groups using a fluorescence microplate reader (Varioskan Flash 3001, Thermo, USA) as previously described [31]. The fluorogenic substrates used for chymotrypsin-like, caspase-like, and trypsin-like activity are Suc-LLVY-AMC, Z-LLE-AMC, and Boc-LRR-AMC, respectively.

2.8. Deubiquitinase (DUB) activity assay

DUB activity was measured as previously reported [25]. Cell lysates (5 μg) and 26S proteasome (25 nM) were incubated with Au(PPh$_3$)PT (0.25, 0.5, 1 μM) or NEM (2 mM) in ice-cold DUB buffer (50 mM Tris-HCl pH 7.5, 5 mM MgCl$_2$, 250 mM sucrose, and 1 mM PMSF) for 15 min. Ub-AMC was then added and the mixtures, at a final volume of 100 μl, were incubated at 25 °C. A fluorescence microplate reader (Varioskan Flash 3001, Thermo, USA) was used to record the release of AMC.

2.9. Active DUB labeling assays

These assays were performed as previously reported [30,31]. Purified 26S proteasomes (25 nM) were incubated with Au(PPh$_3$)PT (2, 20 μM) in DUB buffer for 10 min. HA-UbVS was then added into the mixture for another 1 h at 37 °C. These samples were boiled in the reducing sample buffer and subjected to Western blot analysis. In cells, it was performed as previously reported [25]. A549 or NCI-H1299 cells were either treated with 2 μM, 20 μM Au(PPh$_3$)PT or 50 μM b-AP15 for 2 h, or were treated with 20 μM Au(PPh$_3$)PT, NiPT, CuPT, b-AP15 for 3 h. Whole cell lysates (25 μg) were subsequently incubated with or without HA-UbVS(1 μM) *in vitro* for 30 min at 37 °C. The samples were then subjected to Western blot analysis.

2.10. Nude mouse xenograft model

All animal experiments followed the protocols approved by the Institutional Animal Care and Use Committee of Guangzhou Medical University. Five-week-old male nude Balb/c mice (purchased from Guangdong Animal Center) were subcutaneously inoculated with approximately 1×10^7 A549 or NCI-H1299 cells in a total volume of 100 μl in the left armpit. Seventy-two hours after inoculation, the mice were randomly divided into two groups and treated with either vehicle (DMSO, polyethylene glycol 400, and 0.9% NaCl at 1:3:6 volume ratio) or Au(PPh$_3$)PT (7 mg/kg/day), for a total of 16 days (in A549 xenograft) or 13 days (in NCI-H1299 xenograft). Tumor volumes were determined every three days [27] .

2.11. Immunohistochemical staining

Tumor tissues were fixed, embedded in paraffin and sectioned. Immunohistological staining of tumor xenograft sections (4 μm) was performed using MaxVision TM reagent (MaixinBiol, Fuzhou, China) by following the manufacturer's instructions. After incubation with the primary antibodies, the sections were treated with 0.05% diaminobenzidine and 0.03% H$_2$O$_2$ in 50 mM Tris-HCl (pH 7.6) and counterstained with hematoxylin. Preimmune rabbit serum served as negative control for each antibody.

2.12. ROS measurement

The intracellular reactive oxygen species (ROS) production was detected as previously reported [34]. A549 and NCI-H1299 cells were treated with Au(PPh$_3$)PT (2 μM) and/or NAC (5 mM), tBHQ (100 μM)

for 12 h. Then the cells were washed twice and incubated with serum-free media with the addition of 10 μM of 2′,7′-dichloro-fluorescein diacetate (DCFH-DA) (Keygen, Nanjing, China) for 20 min at 37 °C in the dark. In the presence of ROS, DCFH penetrates the cells and is in turn oxidized to DCF. DCF fluorescence was detected by flow cytometry.

2.13. ALT/AST test

Mouse blood samples were obtained to evaluate the levels of serum ALT and AST. Briefly, blood was collected from mouse hearts, set on bench for 30 min at 25 °C, and then centrifuged at 1800 ×g for 20 min at 4 °C to obtain serum. The serum ALT and AST were measured with the Roche's original kit by a modular analyzer (Roche Cobas 8000, Roche Diagnostics, USA).

2.14. In vitro complex formation of Au(PPh₃)PT with NAC or tBHQ and HPLC analysis.

This was performed as previously reported [34]. A 2 mM solution of Au(PPh₃)PT was mixed with a 500 mM solution of NAC or 100 mM solution of tBHQ, both in DMSO. The mixtures were incubated for 48 h at room temperature and then diluted in methanol before being subjected to HPLC analysis with a Shimadzu dual-pump LC-20AT fitted with a DGU-20A3R. Data was collected digitally with Shimadzu Labsolution software.

2.15. Statistical analysis

All the results were expressed as Mean ± SD, with at least three individual measurements in all experiments. GraphPad Prism 5.0 software (GraphPad Software, USA) was used for statistical analysis. Two-tailed unpaired Student's t-test was used to evaluate the statistical significance of the difference between two groups in all experiments. When the difference among ≥3 groups was evaluated, one-way analysis of variance (one-way ANOVA) was performed. The p <0.05 was considered statistically significant.

3. Results

3.1. Syntheses and structure of the new complex- Au(PPh₃)PT

To synthesize Au(PPh₃)PT, Au(PPh₃)Cl (49 mg, 0.1 mmol) was dissolved in 20 ml of dichloromethane (CH_2Cl_2), followed by the addition of 2-mercaptopyridine-1-oxide sodium(Nampo; 20 mg, 0.1 mmol). The reaction mixture was stirred for six hours before filtration. The resultant filtrates were allowed to evaporate at room temperature for five days. Block-shaped light yellow crystals of complex 1 were collected, washed by ethanol and air-dried, which leads to a yield of 27 mg of Au(PPh₃)PT based on the measurement of Au. Then single crystals of Au(PPh₃)PT was selected for single crystal X-ray analysis. Crystal and structure refinement data for Au(PPh₃)PT was summarized in Table 1, the selected bond distances and angles for Au(PPh₃)PT was listed in Table 2, and the crystal structure of Au(PPh₃)PT was shown in Fig. 1.

3.2. Induction of apoptosis in A549 and NCI-H1299 cells by Au(PPh₃)PT

To determine whether Au(PPh₃)PT has any cytotoxic effects on cancer cells, A549 and NCI-H1299 cells were treated with Au(PPh₃)PT at different concentrations for 24, 48, or 72 h. MTS assay revealed that Au(PPh₃)PT significantly decreased the cell viability in a dose-dependent manner, with the IC_{50} values of 1.41 (24 h), 1.24 (48 h), and 1.02 μM (72 h) in A549 cells; and 1.46 (24 h), 1.22 (48 h), 1.01 μM (72 h) in NCI-H1299 cells, respectively (Fig. 2a, b).

We next determined the time course of Au(PPh₃)PT-induced cell death in these two lung cancer cell lines. Exposure of A549 and

NCI-H1299 cells to Au(PPh₃)PT for 24 h resulted in a dose-dependent increase in AnnexinV/PI-positive cells (Fig. 2c–e). Western blot analysis show a reduction in precursor forms of caspase-3, -8, and -9 with a concomitant increase in the cleaved forms of caspase-3, caspase-8, caspase-9, and PARP after Au(PPh₃)PT treatment in a dose- and time-dependent manner (Fig. 2f, g). These results suggest that Au(PPh₃)PT induces caspase-dependent apoptotic cell death in cancer cells.

3.3. Au(PPh₃)PT inhibits UPS function

We and others have reported that metal complexes can directly inhibit proteasome function [27–31]. To assess whether Au(PPh₃)PT regulates UPS function, we first measured the abundance of ubiquitinated proteins in Au(PPh₃)PT-treated A549 and NCI-H1299 cells. Our results showed that Au(PPh₃)PT resulted in a striking increase in total and K48-linked ubiquitinated proteins in a dose-dependent manner (Fig. 3a). GFPu is a surrogate UPS substrate [35,36], and in HEK293 cells stably expressing GFPu, Au(PPh₃)PT led to the accumulation of GFPu and ubiquitinated proteins (Fig. 3b, c). Notably, the inhibitory effect of Au(PPh₃)PT on the UPS was comparable to Velcade (bortezomib, a classical 20S proteasome inhibitor) [9] and b-AP15 (an inhibitor of 19S proteasomal DUBs) [25] (Fig. 3).

3.4. Au(PPh₃)PT inhibits 19S proteasome-associated DUBs but not 20S proteasome activities

To determine the molecular mechanism by which Au(PPh₃)PT induced proteasome inhibition, we first wanted to know whether Au(PPh₃)PT has any impact on 20S proteasome peptidase activity. By incubating Au(PPh₃)PT with purified 20S proteasome, we observed that Au(PPh₃)PT, even at a dose as high as 20 μM, did not inhibit the caspase-like (C-like), trypsin-like (T-like), and chymotrypsin-like (CT-like) peptidase activities of the purified 20S proteasome, suggesting a distinct function from Vel (Velcade) (Fig. 4a).

We next tested the effect of Au(PPh₃)PT on DUBs activities by measuring the cleavage of a Ub-AMC (ubiquitin 7-amido-4-methylcoumarin), a fluorogenic substrate for a wide range of DUBs, including UCHs and USPs [25]. In cell lysates, Au(PPh₃)PT dose-dependently inhibited the cleavage of Ub-AMC (Fig. 4b). In purified 26S proteasomes, Au(PPh₃)PT completely abrogated the cleavage of Ub-AMC at all of the tested doses, with a potency equivalent to

Table 1
Crystal and structure refinement data for complex Au(PPh₃)PT.

Complex	Au(PPh₃)PT
Empirical formula	$C_{23}H_{19}AuNOPS$
Formula weight	585.39
Crystal system	Monoclinic
Temperature/K	293(2)
Space group	$P2_1/c$
a/Å	10.198(2)
b/Å	12.345(3)
c/Å	17.082(3)
β/(°)	90.02(3)
V/Å³	2086.3(8)
Z	4
Dc/(g·cm⁻³)	1.864
μ/mm⁻¹	15.014
F(000)	1128
Crystal size/mm	$0.2 \times 0.2 \times 0.15$
θ range for data collection/(°)	7.38 to 136.4
Limiting indices	$-12 \leq h \leq 12, -14 \leq k \leq 14, -20 \leq l \leq 20$
Reflections collected	23,432
Independent reflections (Rint)	7439 (0.2396 0.2376)
Observed reflections ($I > 2\sigma(I)$)	4151
Final GOF	1.012
R_1, $_wR_2$ ($I > 2\sigma(I)$)ᵃ	0.1154, 0.2670
R_1, $_wR_2$ (all data)	0.1491, 0.3109
Largest different peak and hole/(e·Å⁻³)	6.04, −1.67

Table 2
Selected bond lengths (nm) and bond angles (°) for complex Au(PPh₃)PT.

Au(1)-P(1)	0.224 24(10)	Au(1)-O(1)	0.257 4(3)	P(1)-C(6)	0.182 1(4)
Au(1)-S(1)	0.231 01(11)	P(1)-C(12)	0.181 9(4)	P(1)-C(18)	0.182 2(4)
P(1)-Au(1)-O(1)	107.74(6)	P(1)-Au(1)-S(1)	176.54(4)	S(1)-Au(1)-O(1)	75.63(7)

N-ethylmaleimide (NEM), a general inhibitor of DUBs (Fig. 4c). We then performed the HA-Ubiquitin-Vinyl Sulfone (HA-UbVS) labeling assay to probe DUB activities. HA-UbVS can covalently bind to the active site of DUBs and the binding affinity reflects the DUBs activity [25]. Like NEM, Au(PPh₃)PT (2 and 20 μM) was able to inhibit the binding of HA-UbVS to both UCHL5 and USP14 in purified 26S proteasome (Fig. 4d). In human A549 and NCI-H1299 cancer cells, low dose (2 μM) Au(PPh₃)PT had negligible effects on HA-UbVs labeling; however, high dose (20 μM) of Au(PPh₃)PT significantly inhibited the binding of HA-UbVs to USP14 and UCHL5, as well as other DUBs. Notably, the inhibitory effect of Au(PPh₃)PT is comparable to the effect of b-AP15, a specific inhibitor of 19S proteasome-associated DUBs [25] (Fig. 4e, f).

Together, our results suggest that Au(PPh₃)PT inhibits 19S proteasome-associated DUBs (UCHL5 and USP14), among others.

3.5. Proteasome inhibition and activation of caspase are attributable to Au(PPh₃)PT-induced cytotoxicity

Given its inhibitory effect on 19S proteasome associated DUBs, we asked whether Au(PPh₃)PT regulates proteasomal proteolytic function. As shown in Fig. 5a, Au(PPh₃)PT treatment at a low dose (2 μM) led to a substantial accumulation of ubiquitinated proteins in both A549 and NCI-H1299 cells, which can be detected as early as 3 h and lasts until 24 h, suggesting that Au(PPh₃)PT inhibits proteasomal proteolytic function. Moreover, the cleavage of PARP, an executor of apoptosis, was not induced until 6 h (in NCI-H1299 cells) or 12 h (in A549 cells) after Au(PPh₃)PT treatment (Fig. 5a), supporting that apoptosis is preceded by proteasome inhibition. To rule out the possibility that the impairment of UPS function is secondary to apoptosis, we tested the effect of pan-
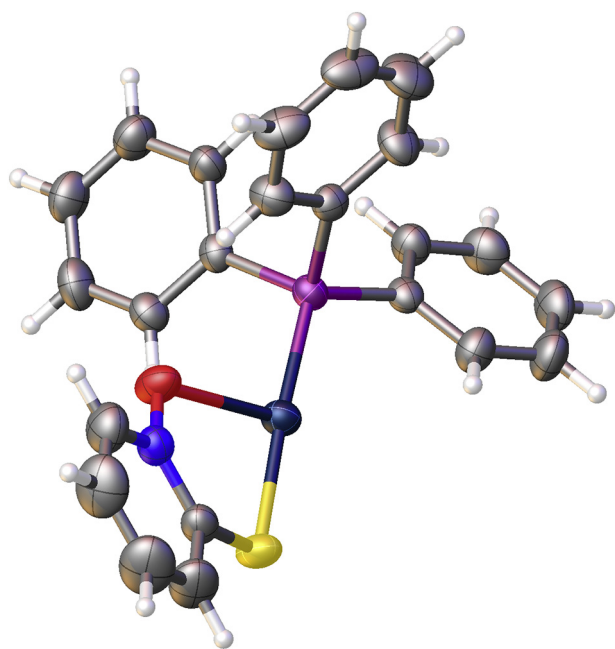
Fig. 1. The crystal structure of Au(PPh₃)PT. Single crystals of Au(PPh₃)PT were scanned by single-crystal X-ray diffraction. The structure of Au(PPh₃)PT was solved using direct methods (SHELXTL) and refined using the full-matrix least-square technique with atomic coordinates and anisotropic temperature factors for all non-hydrogen atoms.

caspase inhibitor z-VAD-FMK on Au(PPh₃)PT-impaired UPS function. As shown in Fig. 5b, while z-VAD-FMK effectively abolished PPAR cleavage, it did not have any effect on Au(PPh₃)PT-induced accumulation of ubiquitinated proteins. These findings suggest that, like other classic proteasome inhibitors [32,37], Au(PPh₃)PT inhibits UPS proteolytic function and induces caspase-dependent apoptosis.

Next, we found that like other gold containing compounds [38], Au(PPh₃)PT increased ROS (reactive oxygen species) production in A549 and NCI-H1299 cells, which was attenuated by ROS scavenger NAC (N-acetyl-cysteine) and tert-Butylhydroquinone (tBHQ) (Fig. 5c, d). Interestingly, NAC, but not tBHQ, was able to effectively reverse Au(PPh₃)PT-induced proteasome inhibition and apoptosis as evidenced by the reduction in ubiquitinated proteins and PARP cleavage (Fig. 5e). We further found that NAC, but not tBHQ, altered the chemical structure of Au(PPh₃)PT (Fig. S1). These results suggest that proteasome dysfunction but not ROS production plays a major role in Au(PPh₃)PT-induced cell death.

### 3.6. Au(PPh₃)PT inhibits proteasome function and induces cytotoxicity in cancer cells from leukemia patients

Proteasome inhibitors have been proven effective in treating leukemia patients [8,9]. Thus we sought to determine the ex vivo antineoplastic effect of Au(PPh₃)PT using monocytes isolated from 7 patients with AML and 6 healthy volunteers. As shown in Fig. 6a, primary monocytes from AML patients were more sensitive to Au(PPh₃)PT-induced cell death, as evidenced by much lower IC₅₀ values (ranging from 0.66 to 5.091 with an average of 2.02 μM) than normal controls (ranging from 2.83 to 15.87 μM with an average of 10.63 μM). As expected, the proteasome inhibitor Velcade caused more cell death in monocytes isolated from AML patients than in those from healthy controls (Fig. 6b). Consistently, Annexin V/PI staining followed by flow cytometry analysis revealed that 1 μM of Au(PPh₃)PT only caused cell death in ~20% of monocytes isolated from healthy controls (Fig. 6c, d); while it significantly induced cell death in ~85% of monocytes isolated from AML patients (Fig. 6f, g). Moreover, Au(PPh₃)PT drastically increased the levels of total and K48-linked ubiquitinated proteins in the monocytes isolated from AML patients (Fig. 6h); however, the same doses had much less robust effects in the monocytes from normal controls (Fig. 6e). These ex vivo results demonstrate that monocytes from AML patients are more susceptible to Au(PPh₃)PT-induced cell death, likely due to increased sensitivity to proteasome inhibition .

3.7. Au(PPh₃)PT inhibits proteasome function and tumor growth in vivo

We next wanted to assess the antineoplastic action of Au(PPh₃)PT in vivo. Xenograft models were created by subcutaneous injection of A549 or NCI-H1299 cells to immunodeficient BALB/c nude mice. Three days after inoculation, these mice were treated with vehicle or Au(PPh₃)PT (7 mg/kg/day) via intraperitoneal injection for up to 16 days in A549, and 13 days in NCI-H1299 xenograft, respectively. Au(PPh₃)PT significantly inhibited tumor growth in both models, as evidenced by significantly decreased tumor size (Fig. 7a, b, e, f). Moreover, Au(PPh₃)PT treatment led to ~42.5% reduction of tumor weight in A549 xenograft model and ~46.1% reduction in NCI-H1299 xenograft model (Fig. 7c, g). Despite its tumor-suppressive effect, Au(PPh₃)PT treatment did not cause significant body weight loss (Fig. S2). Immunohistochemistry staining revealed that total ubiquitinated proteins were
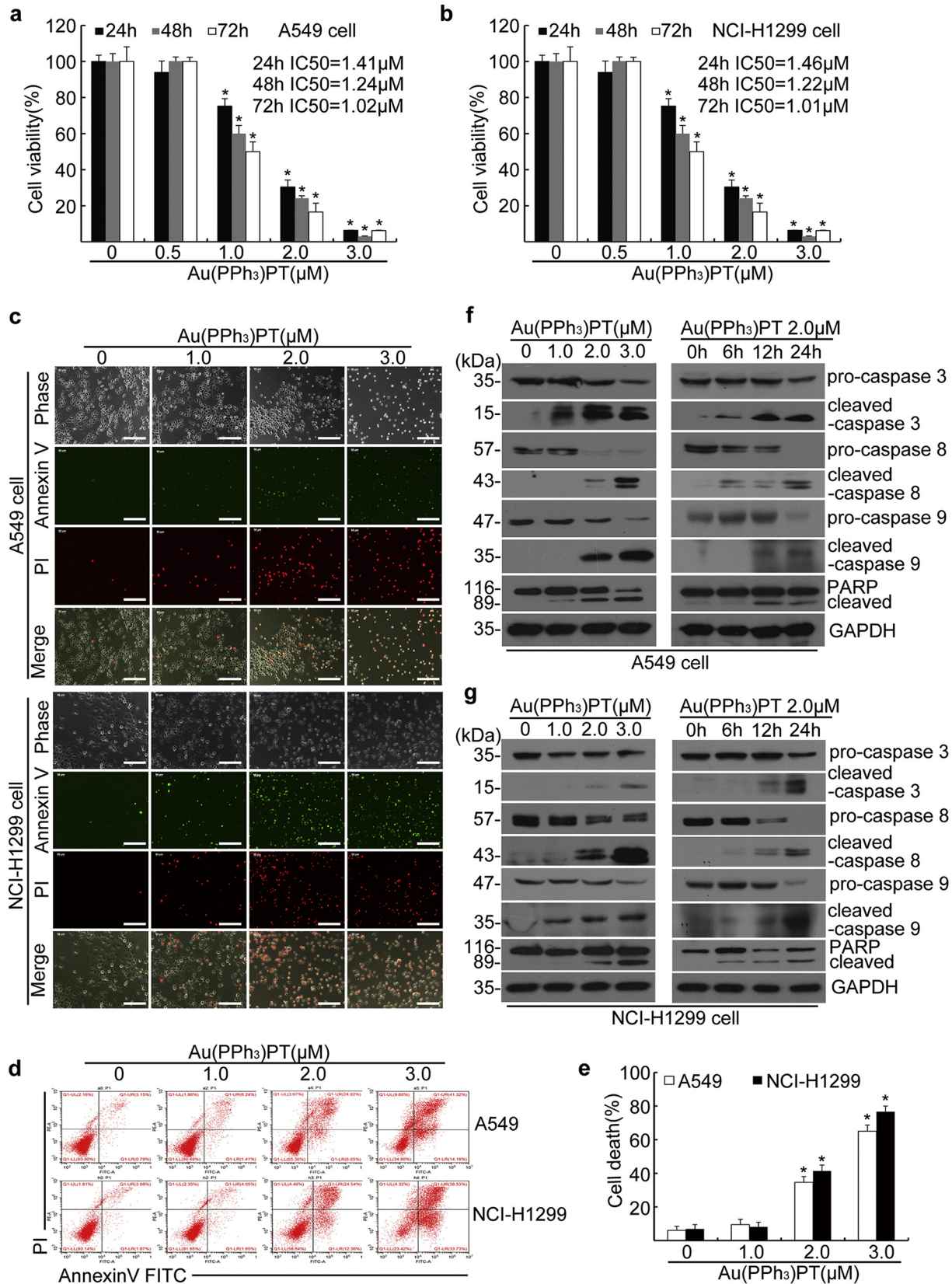
Fig. 2. Au(PPh$_3$)PT induced cytotoxicity in A549 and NCI-H1299 lung cancer cell lines. A549 and NCI-H1299 cells were treated with Au(PPh$_3$)PT at the indicated concentrations at different time points (a, b, f, and g) or 24 h (c-e). (a, b) Viability of A549 and NCI-H1299 cells assessed by MTS assay. Data from three biological repeats are presented. Mean ± SD ($n = 3$). (Two-tailed unpaired Student's t-test) *P <0.05 *versus* control. (c-e) Apoptotic cells were detected by Annexin V-FITC/PI staining, followed by microscopy and flow cytometry analysis. Representative microscopic images (bars, 200 μm) (c), flow cytometry analysis (d), and the quantitative data from flow cytometry (e) are shown. Mean ± SD ($n = 3$). (Two-tailed unpaired Student's t-test) *P <0.05 *versus* control. (f, g) Western blot analysis of indicated proteins in A549 (f) and NCI-H1299 (g) cells. GAPDH serves as loading control.
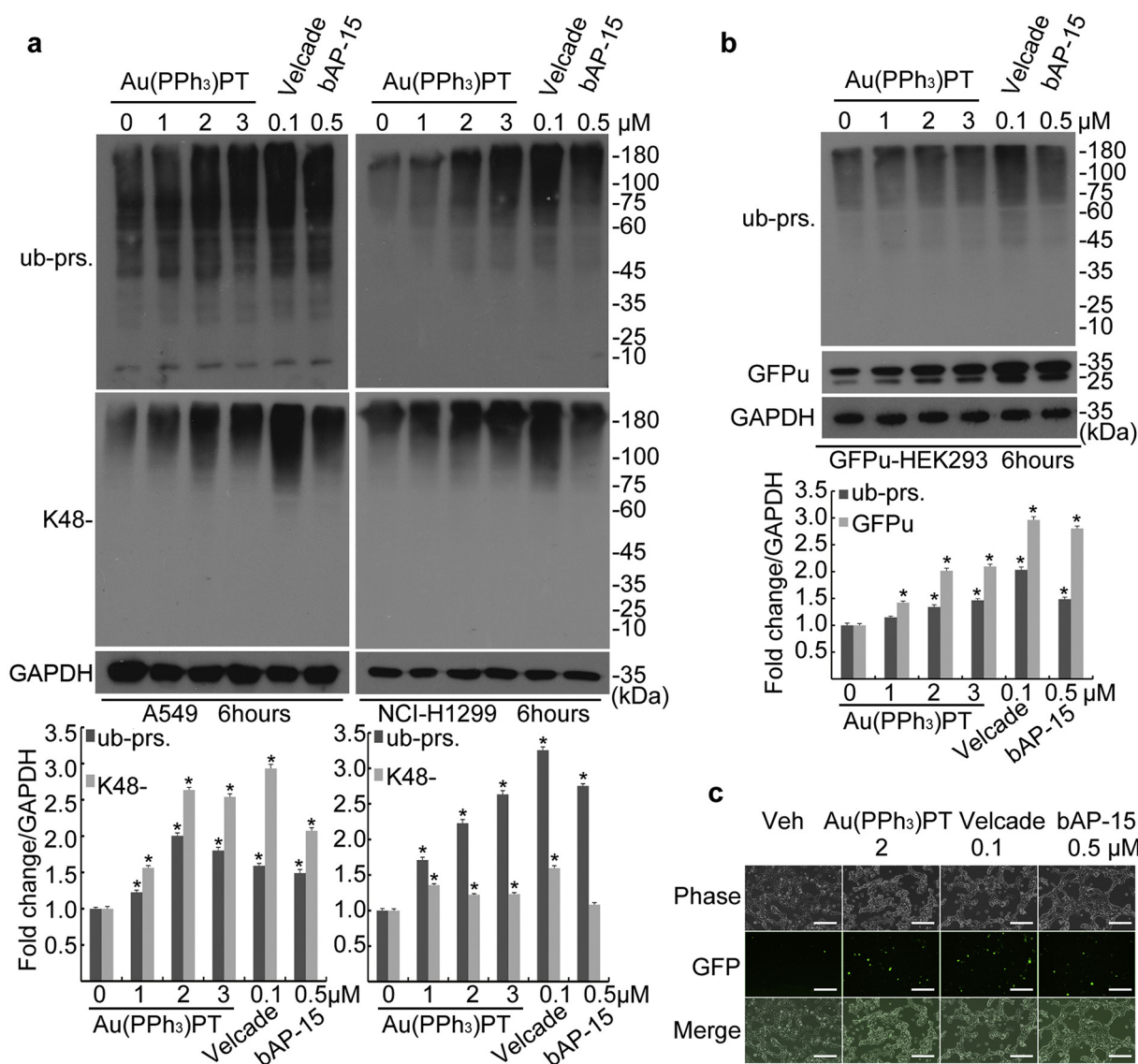
Fig. 3. Au(PPh₃)PT inhibits UPS function in cultured cells. (a) A549 (left) and NCI-H1299 (right) cells were treated with various concentrations of Au(PPh₃)PT for 6 h. Western blot analysis of total ubiquitinated proteins (Ub-prs.) and K48-linked ubiquitinated proteins (K48-) is shown. GAPDH serves as loading control. Velcade (0.1 μM) and b-AP15 (0.5 μM) were used as positive controls of proteasome inhibition. Grey-scale analysis of the indicated proteins by ImageJ software. All data are expressed as Mean ± SD ($n = 3$). (Two-tailed unpaired Student's t-test) *$P < 0.05$ versus control. (b, c) HEK293 cells stably expressing GFPu, a UPS surrogate substrate, were treated with Velcade (0.1 μM), b-AP15 (0.5 μM), or Au(PPh₃)PT at the indicated concentrations for 6 h. Western blots of the indicated proteins (b) and representative bright field (Phase) and fluorescent (GFP) images (bars, 200 μm) (c) are shown. Grey-scale analysis of the indicated proteins in (b) was performed as in (a). Mean ± SD ($n = 3$). (Two-tailed unpaired Student's t-test) *$P < 0.05$ versus control.

significantly increased, while Ki67-positive cells, a nuclear non-histone protein that is associated with cell proliferation [39], were significantly decreased in the Au(PPh₃)PT-treated tumors (Fig. 7d, h). Meanwhile, the activity of cleaved-caspase 3 and 8 increased both in A549 and NCI-H1299 xenograft mice (Fig. S3). Together, these results demonstrate that Au(PPh₃)PT has strong inhibitory effects on both proteasome function and tumor growth in vivo.

3.8. Au(PPh₃)PT has cellular functions distinct from other metal compounds

We have reported that other metal complexes (NiPT and CuPT) suppressed tumor growth via targeting proteasome function [27–31]. We wanted to gain new insights into the molecular actions and efficacy of these complexes in comparison to Au(PPh₃)PT. We first compared their effects on the viability of cancer cells (A549, NCI-H1299) and normal cells (human epithelial lung cell line BEAS-2B). As shown in Fig. 8a–8c, CuPT has comparable IC₅₀ in cancer cells (0.12 μM in A549 and 0.28 μM in NCI-H1299) and in normal cells (0.24 μM in BEAS-2B),

suggesting that CuTP has little selectivity on inhibiting cancer cell growth. In contrast, Au(PPh₃)PT (IC₅₀ = 4.22 μM) and NiPT (IC₅₀ = 7.84 μM) exerted a much lower cytotoxicity in BEAS-2B cells compared with CuPT. While Au(PPh₃)PT has a slightly higher cytotoxicity on normal cells compared with NiPT, it is more potent in inducing cell death in cancer cells (IC₅₀ = 1.36 μM vs. 6.80 μM of NiPT in A549 cells and IC₅₀ = 1.31 μM vs. 4.92 μM of NiPT in H1299 cells). These findings suggest that Au(PPh₃)PT has a higher selectivity in inhibition of cancer cell growth.

We next compared the inhibitory effects of these metal compounds on DUB activities by performing the HA-UbVS labeling assay in A549 and NCI-H1299 cancer cells. The results show that at the same dose (20 μM), Au(PPh₃)PT and CuPT had inhibitory effects equivalent to that of b-AP15 on the binding of HA-UbVs to USP14 and UCHL5, as well as other DUBs (USP7, USP10, USP15, USP25). In contrast, NiPT show less inhibition on the activity of USP14, and has no effect on other tested DUBs activity (Fig. 8d). Thus, these data support that Au(PPh₃)PT is a specific pan-inhibitor of DUBs among the tested metal compounds.
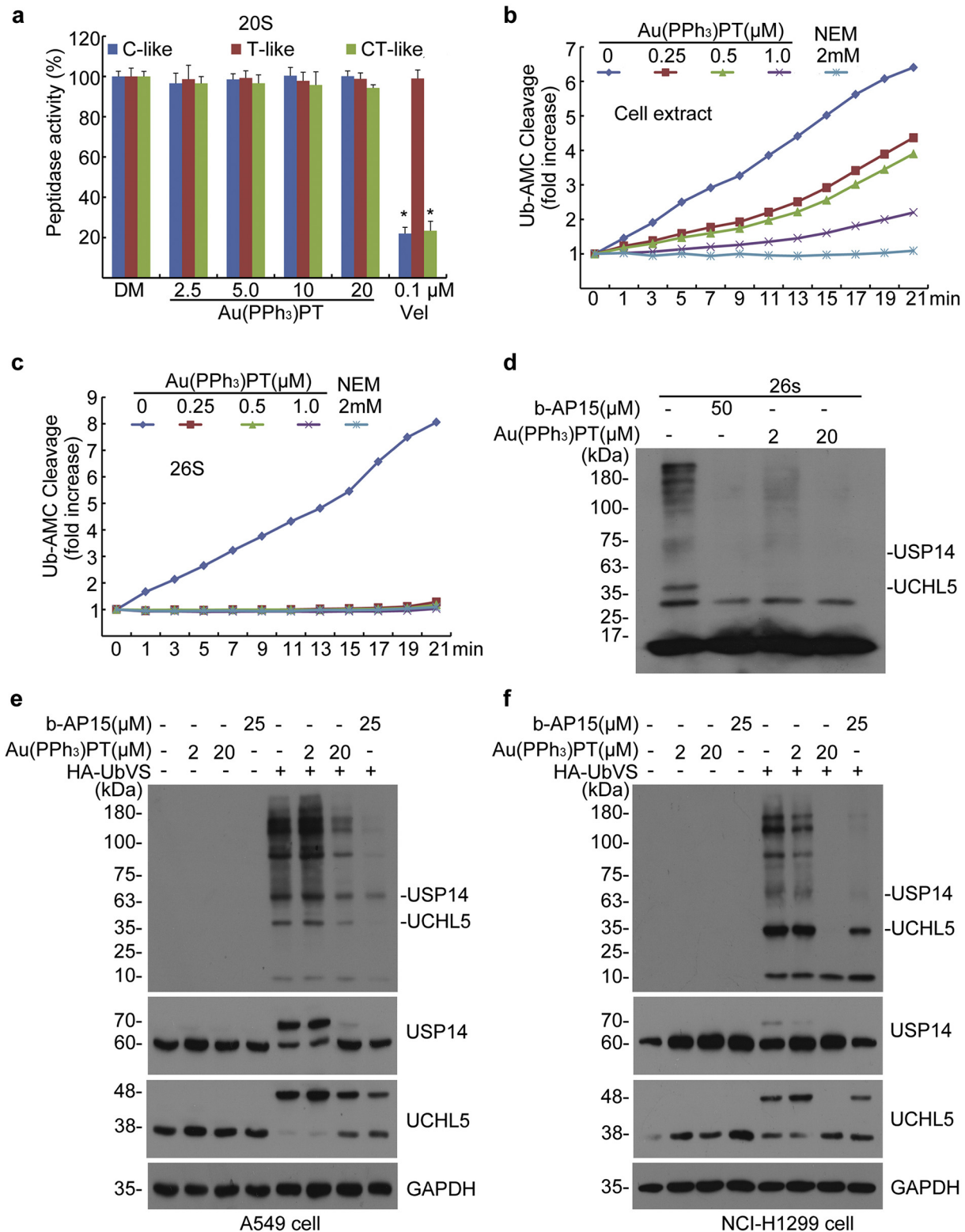
Fig. 4. Au(PPh₃)PT inhibits proteasome deubiquitinase activities. (a) Au(PPh₃)PT did not alter 20S proteasome peptidase activities. Purified 20S proteasomes were treated with DMSO (DM) or Au(PPh₃)PT at the indicated doses. The caspase-like (C-like), trypsin-like (T-like), and chymotrypsin-like (CT-like) peptidase activities were measured using specific synthetic fluorogenic substrates. Velcade (Vel, 0.1 μM) was used as a positive control. Mean + SD ($n = 3$). (Two-tailed unpaired Student's t-test) *P <0.05 *versus* DM. (b) Effects of Au(PPh₃)PT on the cleavage of Ub-AMC in cell lysate. Cell lysate was treated with the indicated doses of Au(PPh₃)PT or NEM (N-ethylmaleimide, 2 mM) for 15 min prior to incubation with Ub-AMC. DUB activity was expressed as fold change of fluorescence units (RFU) relative to the at the start point reading. Shown is a representative image of three independent repeats. (c) Effects of Au(PPh₃)PT on the cleavage of Ub-AMC. Purified 26S proteasomes were treated with the indicated doses of Au(PPh₃)PT or NEM (2 mM). DUB activity was measured as described in (b). (d) Active-site-directed labeling of proteasomal DUBs. 26S proteasomes were treated with Au(PPh₃)PT (2 or 20 μM) for 10 min and then labeled with HA-UbVS for 1 h at 37 °C. Western blots are shown. b-AP15 (50 μM) was used as a positive control for DUB inhibition. (e, f) Au(PPh₃)PT inhibited the binding of HA-UbVS to the active sites of proteasomal deubiquitinases. A549 (e) and NCI-H1299 (f) cells were treated with 2 μM or 20 μM Au(PPh₃)PT for 2 h. Cell lysates were subsequently labeled with or without HA-UbVS (1 μM) *in vitro* for 30 min at 37 °C. Western blots of the indicated proteins are shown.
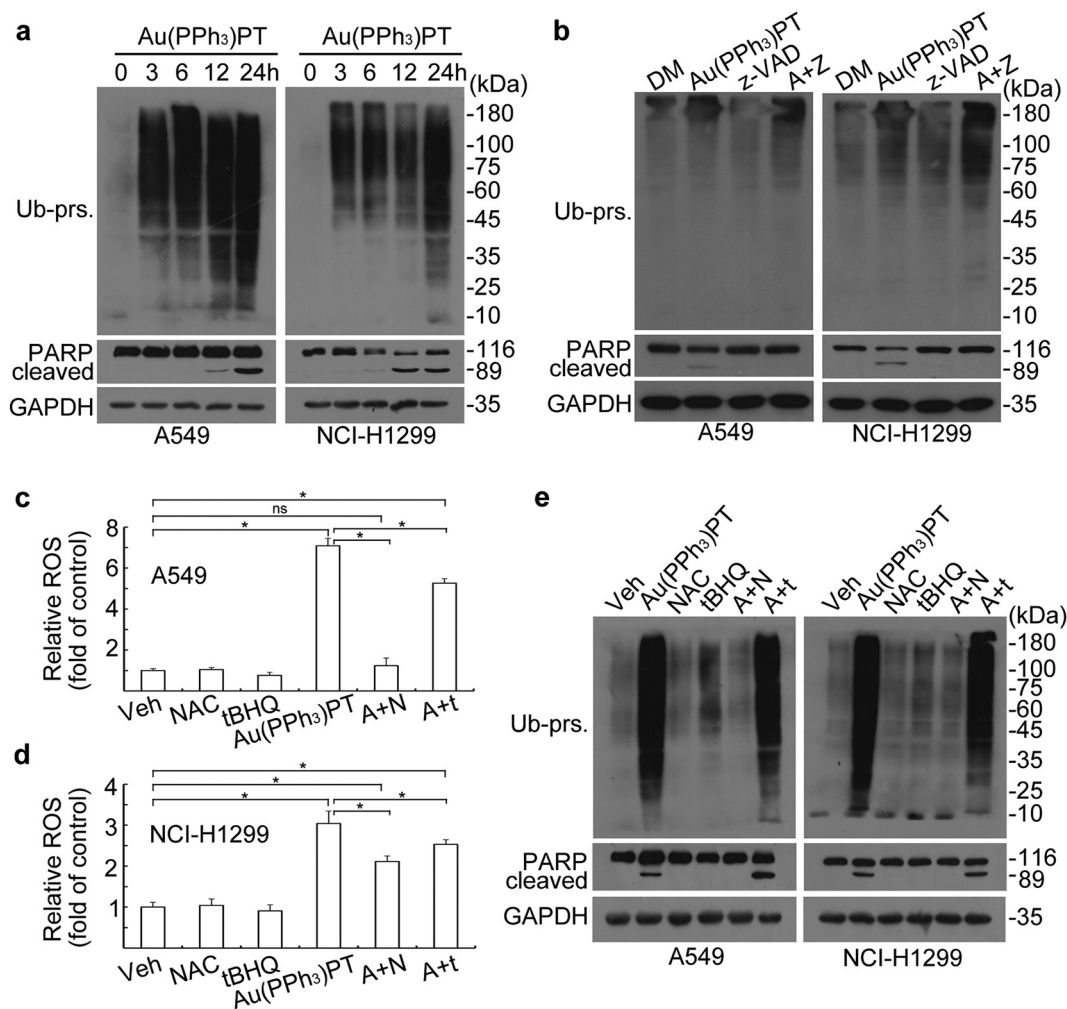
Fig. 5. Proteasome inhibition precedes the activation of caspase in Au(PPh₃)PT-treated cells. (a) The time-course effect of Au(PPh₃)PT on proteasome activity and apoptosis. A549 (left) and NCI-H1299 (right) cancer cells were treated with Au(PPh₃)PT (2 μM) for the indicated times. Western blots of indicated proteins are shown. GAPDH serves as loading control. (b) A549 (left) and NCI-H1299 (right) cells were treated with Au(PPh₃)PT (2 μM) and/or z-VAD-FMK (50 μM) for 12 h. Total ubiquitinated proteins (Ub-prs.) and PARP proteins were assessed by Western blot. GAPDH was serves as loading control. (c, d) NAC and tBHQ attenuated Au(PPh₃)PT-induced ROS generation. A549 (c) and NCI-H1299 (d) cells were treated with Au(PPh₃)PT (2 μM), NAC (5 mM), tBHQ (50 μM), Au(PPh₃)PT + NAC (A + N), or Au(PPh₃)PT + tBHQ (A + t) for 12 h. ROS was detected by flow cytometry. Relative level of ROS are shown. Mean ± SD (n = 3). (One-way ANOVA with Tukey's test) *P<0.05; ns, not significant. (e) NAC reversed Au(PPh₃)PT-induced accumulation of ubiquitinated proteins and PPAR cleavage. A549 and NCI-H1299 cells were treated as in (c, d). Western blot analyses for the indicated proteins were performed.

We also compared the effect of these metal compounds on the DNA damage response pathway. We found that CuPT, but not Au(PPh₃)PT and NiPT, significantly increased the levels of DNA damage-related proteins including p-ATM, p-CHK1, p-CHK2, and γ-H2AX in both cancer cells (A549) and normal cells (BEAS-2B) (Fig. 8e), suggesting that Au (PPh₃)PT and NiPT do not induce DNA damage *in vitro*. In addition, we injected Balb/c mice with the same dose of Au(PPh₃)PT, NiPT, and CuPT (2 mM/kg/day for 7 days, i.p.) and measured the activity of alanine aminotransferase (ALT) and aspartate aminotransferase(AST), two enzymes indicative of liver function, in the plasma. The results showed that CuPT treatment significantly increased the level of ALT/AST in the plasma (Fig. 8f, g), indicating that CuPT induced hepatic stress in mice.

4. Discussion

DUBs, especially 19S proteasome-associated DUBs are increasingly being recognized as potential drug targets for cancer therapies. Although inhibitors of proteasomal DUBs have recently been developed and are able to suppress tumor growth under experimental settings [40], their effectiveness in cancer patients remains to be tested in clinical studies. Additionally, metal-based compounds have recently gained attention for their potential as proteasome inhibitors in cancer therapy.

In the present study, we developed a new gold(I) complex, Au(PPh₃)PT, that possesses potent anti-tumor activities both *in vitro* and *in vivo*. We further demonstrated that Au(PPh₃)PT inhibits UPS function by targeting 19S proteasome-associated DUBs (UCHL5 and USP14) and other non-proteasome DUBs (USP7, USP10, USP15, and USP25). Hence, this study identifies a novel DUB inhibitor that may have potential use in cancer treatment.

In the past decade, chemical complexes containing metal ions including, but not limited to, gallium (III), copper (II), zinc (II), nickel (II), and cobalt (II) were targeted to inhibit the 26S proteasome [41–45]. The discovery of these metal-based compounds provides a new direction in developing novel anticancer drugs. Although several metal-based compounds have been reported to inhibit UPS function, their potency in limiting tumor growth in patients remains to be demonstrated. While cisplatin has been commonly used for treatment of several types of solid tumors, its clinical application has been associated with severe side effects: drug resistance and reoccurrence of malignancies [33]. Therefore, substantial efforts have been directed to search for novel non-platinum-containing metal compounds with potent anti-cancer activity but low toxicity. We and others have reported that several gold-containing compounds can directly inhibit 20S proteasome peptidase activities. Specifically Auranofin (Aur), a gold (I)-containing
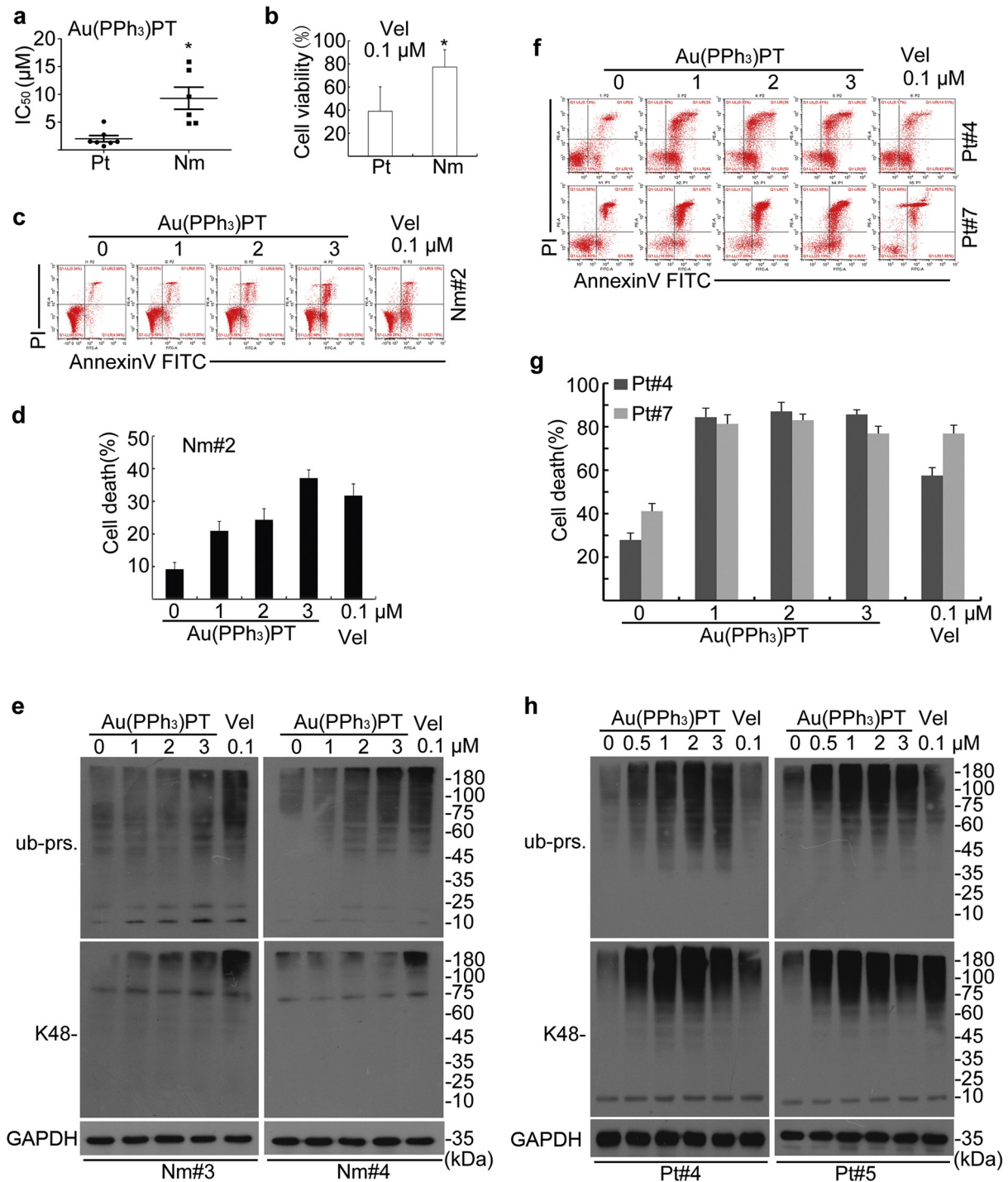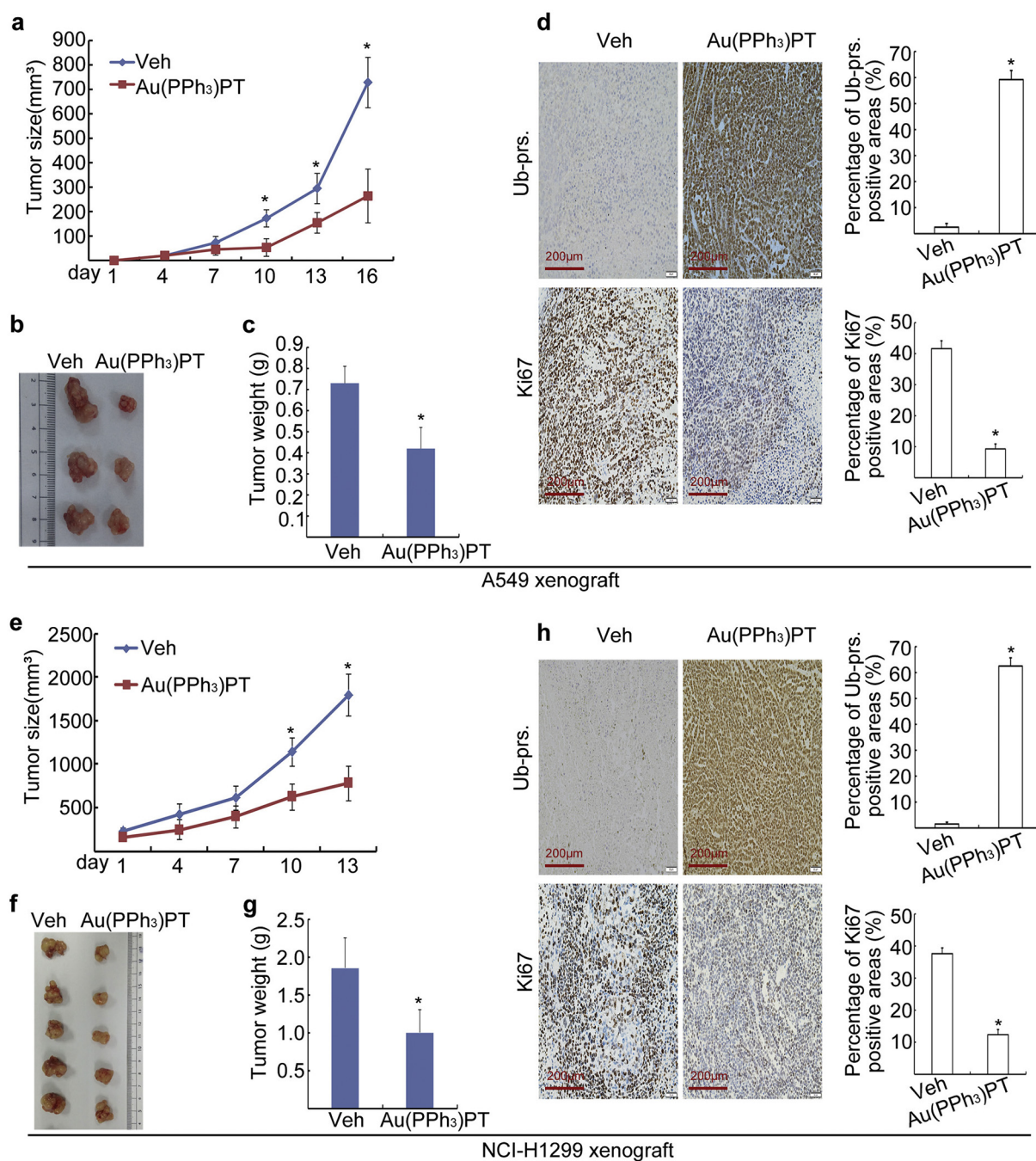
Fig. 6. Au(PPh$_3$)PT inhibited proteasomal function and specifically induced cytotoxicity in cancer cells from acute myeloid leukemia (AML) patients. (a, b) Cancer cells from 7 AML patients (Pt) and peripheral blood mononuclear cells from 6 healthy volunteers were treated with Au(PPh$_3$)PT at the indicated doses or with Velcade (Vel, 0.1 μM) for 24 h. Cell viability was determined by MTS assay. The IC$_{50}$ values in each group are shown in the scatter plot (a). Mean ± SD (n = 7 or 6). (Two-tailed unpaired Student's t-test) *P <0.05, *versus* patients. Cell viability with Vel treatment in each group is shown in (b). Mean ± SD (n = 7 or 6). (Two-tailed unpaired Student's t-test) *P <0.05, *versus* AML patients. (c-e) Peripheral mononuclear cells from healthy volunteers were incubated with Au(PPh$_3$)PT at the indicated doses or with Vel (0.1 μM) for 24 h. Cell death was detected by Annexin V/PI staining, followed by flow cytometry (c). Quantification results are summarized in (d). Western blots of the indicated proteins are shown in (e). GAPDH serves as loading control. (f-h) AML cancer cells were treated with the indicated doses of Au(PPh$_3$)PT or Vel (0.1 μM)) for 24 h. Cell death were detected by Annexin V/PI staining and analyzed by flow cytometry. Representative images (f) and the quantification (g) are shown. Western blots of the indicated proteins are shown in (h).

compound that has been widely used to alleviate the symptoms of rheumatic arthritis, was found to be a potent inhibitor of 19S proteasome-associated DUBs (UCHL5 and USP14) [34,46]. Furthermore, we have found that several metal complexes of pyrithione (PT) inhibit proteasome peptidase activity and trigger cell death in cancer cells [27,30,31]. Since PT possesses excellent metal chelating properties, we

sought to synthesize a new gold(I) complex of pyrithione, Au(PPh$_3$) PT, and to investigate its potential anti-tumor effects.

The current study demonstrates that Au(PPh$_3$)PT is a novel inhibitor of UPS function. It is generally believed that lysine 48 (K48)-linked ubiquitinated proteins are preferable substrates for the proteasome *versus* other linkages [47]. Using K48-linked proteins, total

Fig. 7. Au(PPh₃)PT inhibited tumor growth and impaired the proteasome function of tumor xenografts in nude mice. BALB/c nude mice bearing A549 and NCI-H1299 tumors were treated with vehicle (Veh) or Au(PPh₃)PT (7 mg/kg/day, i.p.) for 16 (A549) and 13 (NCI-H1299) days, respectively. Tumor growth curves were recorded every three days. Tumor size (a, e), tumor images (b, f), and tumor weight (c, g) are shown. Mean ± SD (n = 6). (Two-tailed unpaired Student's t-test) *P <0.05. (d, h) Immunohistochemistry staining of total ubiquitinated proteins (Ub-prs.) and Ki67 in tumor tissues. Representative images collected at a magnification of 200× are shown. The level of Ub-prs. and Ki67 were quantitated by ImageJ software. n = 3 mice per treatment, Mean ± SD. (Two-tailed unpaired Student's t-test) *P <0.05, compared with Vehicle control.

polyubiquitinated proteins, and GFPu as readouts, we show that Au(PPh₃)PT can lead to the accumulation of both endogenous and exogenous proteasome substrates *in vitro*, *ex vivo* and *in vivo* (Fig. 3, 6h, 7d, h). Notably, therapeutic doses of Au(PPh₃)PT are sufficient to inhibit UPS at a potency comparable to Vel (Fig. 3). We further prove that, in contrast to Vel, Au(PPh₃)PT did not inhibit the caspase-like, trypsin-like, or chymotrypsin-like activities of 20S proteasomes (Fig. 4a), suggesting that Au(PPh₃)PT does not target 20S proteasome.

Next we demonstrate that 19S proteasome-associated UCHL5 and USP14 are likely directly targeted by Au(PPh₃)PT. By detecting the cleavage of Ub-AMC and HA-UbVs labeling, we showed that Au(PPh₃)PT has robust effects on inhibiting the activities of UCHL5 and USP14, two 19S proteasome associated DUBs, in both purified 26S proteasomes and in cancer cells (Fig. 4). Due to the lack of a reliable readout, it remains unclear whether Au(PPh₃)PT targets RPN11, an intrinsic 19S proteasome DUB that is required for 26S proteasome-mediated proteolysis. Inhibition of USP14 has been shown to promote proteasomal proteolytic function [48]. Therefore, it is very likely that the impairment of UPS function by Au(PPh₃)PT is an outcome of the combined effects of USP14 and UCHL5 inhibition.

Previous studies have indicated that blockade of tumor proteasome activity results in cancer cell apoptosis [49], and that gold (I)-containing
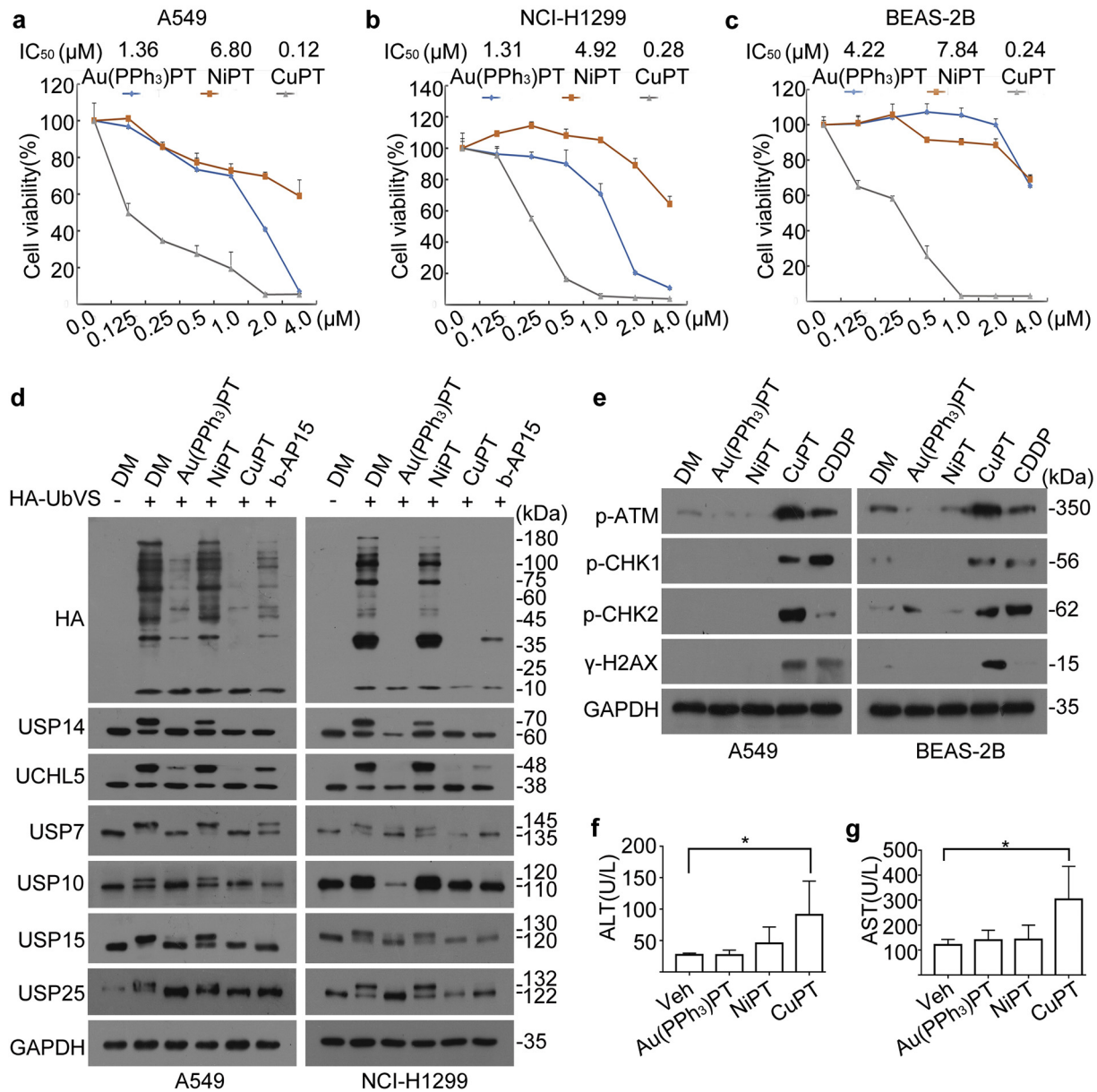
Fig. 8. DUB activity inhibition and cytotoxicity induced by Au(PPh$_3$)PT compared to other metal complexes. (a, b, c) Cytotoxic curves of the indicated metal complexes. Cancer cells A549 (a) and NCI-H1299 (b), and human epithelial lung cell BEAS-2B (c) were treated with escalating doses of Au(PPh$_3$)PT, NiPT, or CuPT for 24 h. Cell viability was measured by MTS assay. Values are expressed as Mean ± SD ($n = 3$). The IC$_{50}$ values of the complexes are shown. (d) The effects of Au(PPh$_3$)PT, NiPT, or CuPT on the binding of HA-UbVS to the active sites of DUBs. A549 (left) and NCI-H1299 (right) cells were treated with Au(PPh$_3$)PT (20 μM), NiPT (20 μM), or CuPT (20 μM) for 3 h. Cell lysates were subsequently labeled with HA-UbVS (1 μM) *in vitro* for 30 min at 37 °C. Western blots of the indicated proteins are shown. b-AP15 (20 μM) serves as positive control for DUB inhibition. GAPDH was used as a loading control. (e) Western blot of DNA damage-related proteins in A549 and BEAS-2B cells treated with Au(PPh$_3$)PT (2 μM), NiPT (2 μM), or CuPT (2 μM) for 3 h. CDDP (10 μM) was used as positive control for DNA damage response. (f, g) The activities of alanine aminotransferase (ALT) and aspartate aminotransferase(AST) in mouse serum. BALB/c mice were injected with vehicle (Veh), Au(PPh$_3$)PT, NiPT, or CuPT (2 mM/kg/day, i.p.) for 7 days and the sera were collected for ALT/AST tests. Values are expressed as Mean ± SD ($n = 5$). (Two-tailed unpaired Student's t-test) *P <0.05, compared with Vehicle control.

compound, Aur, induced intracellular ROS generation [38]. Consistent with these reports, we found that cleaved PARP (an apoptosis indicator) was preceded by proteasome inhibition in Au(PPh$_3$)PT-treated cancer cells (Fig. 5a). The new gold(I) complex of pyrithione, Au(PPh$_3$)PT, also increased ROS production in cancer cell lines A549 and NCI-H1299 (Fig. 5c, d). Interestingly, while both thiol-containing anti-oxidant (NAC) and phenol-containing antioxidant (tBHQ) effectively scavenged Au(PPh$_3$)PT-induced ROS production (Fig. 5c, d), only NAC completely prevented Au(PPh$_3$)PT-induced total polyubiquitinated proteins accumulation and PARP cleavage (Fig. 5e) because NAC alone alters the chemical structure of Au(PPh$_3$)PT (Fig. S1). Taken together, these results indicate that UPS dysfunction, rather than ROS production, plays a major role in Au(PPh$_3$)PT-induced cell death.

Cancer cells rely on hyperactive proteasomes to offset proteotoxicity resulting from metabolic, hypoxic, and mechanical stress, and therefore are highly sensitive to UPS inhibitors. We presented *in vitro*, *ex vivo*, and *in vivo* evidence demonstrating the selective anticancer activity of Au(PPh$_3$)PT (Figs. 2, 6, 7), which is at least in part attributable to the inhibition of UPS function and the induction of apoptotic cell death. Besides targeting 19S proteasome-associated DUBs, Au(PPh$_3$)PT can also diminish the activity of other cytoplasmic non-proteasomal DUBs, including USP7, USP10, USP15, and USP25 (Fig. 4, 8d), which may also contribute to its cytotoxicity in cancer cells. Interestingly, previous studies have revealed both oncogenic and tumor suppressive functions of these DUBs. On the one hand, inhibition of USP7 increased tumor suppressor INK4a and caused senescence [50]. USP15 stabilized TGFβ receptor I and

promoted oncogenesis in glioblastoma [51]. Silencing of USP25 was shown to inhibit invasion and metastasis of human non-small cell lung cancer [52]. On the other hand, downregulation of USP10 associated with tumorigenesis possibly through promoting the degradation of tumor suppressors such as P53 and SIRT6 [53,54]. Therefore, the tumor suppressive effects of Au(PPh$_3$)PT is likely the combinational outcome of its inhibition on both oncogenic and tumor suppressive DUBs. Nevertheless, the specificity of Au(PPh$_3$)PT on these DUBs, as well as the mechanisms by which Au(PPh$_3$)PT inhibits DUBs, remains to be understood. Au(PPh$_3$)PT elicits robust cytotoxicity in bone marrow cells from AML patients but induces much less cytotoxicity in monocytes from healthy volunteers (Fig. 6). Moreover, Au(PPh$_3$)PT treatment did not cause body weight loss (Fig. S2) and hepatic injury (Fig. 8f, g) in mice at the doses required to repress tumor growth, indicating the lack of systematic toxicity. Together, our study identifies a new metal-based compound as a promising anticancer drug.

We have previously reported that several metal-based compounds exert anti-tumor activity. CuPT, a chelating product of copper ion and pyrithione, suppresses tumor growth by targeting both 19S proteasome-specific DUBs and 20S proteasome peptidases [27]. A nickel complex, NiPT, is also effective in restraining tumor growth by inhibiting the 19S proteasomal DUBs USP14 and UCHL5 (Zhao et al., 2016). Our comparison analysis of these compounds (Fig. 8) showed that CuPT induced DNA damage and cell death equivalently in cancer cells and normal cells and led to liver injury in mice, suggesting that targeting both 20S proteasome and DUBs by CuPT is quite toxic to normal cells. In contrast, inhibition of DUBs by either NiPT or Au(PPh$_3$)PT appeared to be more tolerable by normal cells and does not cause DNA damage in cultured cells or liver injury in mice. Moreover, Au(PPh$_3$)PT exhibits higher potency in inducing cell death in cancer cells compared with NiPT (Fig. 8a, b), possibly owing to its broad effect in inhibiting both 19S proteasome-associated DUBs and other cytoplasmic DUBs. Interestingly, we found that b-AP15, a specific inhibitor of 19S proteasome-associated DUBs (USP14 and UCHL5) [25], like Au(PPh$_3$)PT, also inhibited other non-proteasomal DUBs (USP7, USP10, USP15, USP25) (Fig. 8d), warranting further investigation. Our finding suggested that different metal complexes have distinct actions in inhibition of UPS function and tumor growth.

Besides metal-based compounds, a new class of compounds that target proteasomal DUBs have recently been developed to inhibit tumor growth [25,55–58]. For instance, RA-9 inhibits not only 19S proteasome DUBs (USP14 and UCHL5) but also other cytoplasmic DUBs such as UCHL1, UCHL3, USP8, and USP9x in vitro. WP1130 was found to inhibit a broad spectrum of DUBs, whereas IU1 selectively inhibits USP14 but not UCHL5 activity [48]. Our studies, along with others, suggest that targeting 19S proteasome DUBs and other cytoplasmic DUBs could be a promising strategy for cancer therapy.

In conclusion, we identify a novel metal-containing compound, Au(PPh$_3$)PT, that exhibits strong inhibitory effect on the growth of multiple cancer cell types in vitro, ex vivo, and in vivo. Mechanistically, Au(PPh$_3$)PT inhibits 19S proteasome-associated DUBs and other non-proteasomal DUBs, leading to the severe impairment of UPS function and consequent prevalent apoptotic cell death. Thus, Au(PPh$_3$)PT is a promising anti-cancer drug candidate. Further investigation is warranted to confirm its preclinical and clinical value in the field of cancer therapy.

Supplementary data to this article can be found online at https://doi.org/10.1016/j.ebiom.2018.11.047.

Conflicts of interest

The authors confirm that there are no conflicts of interest.

Author contributions

Jinbao Liu and Xiaofen Li designed experiments; Peiquan Zhang synthesized the new complex and determined the structure of compound; Xiaofen Li, Qingtian Huang,Huidan Long, and Peiquan Zhang performed laboratory experiments; Jinbao Liu and Huabo Su wrote and revised the manuscript. All authors were involved in editing and approval of the final manuscript. Xiaofen Li, Qingtian Huang, and Huidan Long contributed equally to this work.

References

[1] Adams J. The proteasome: structure, function, and role in the cell. Cancer Treat Rev 2003;29(Suppl. 1):3–9.
[2] de Pril R, Fischer DF, van Leeuwen FW. Conformational diseases: an umbrella for various neurological disorders with an impaired ubiquitin-proteasome system. Neurobiol Aging 2006;27(4):515–23.
[3] Tran K, Mahr JA, Spector DH. Proteasome subunits relocalize during human cytomegalovirus infection, and proteasome activity is necessary for efficient viral gene transcription. J Virol 2010;84(6):3079–93.
[4] Finley D. Recognition and processing of ubiquitin-protein conjugates by the proteasome. Annu Rev Biochem 2009;78:477–513.
[5] Su H, Wang X. The ubiquitin-proteasome system in cardiac proteinopathy: a quality control perspective. Cardiovasc Res 2010;85(2):253–62.
[6] Burger AM, Seth AK. The ubiquitin-mediated protein degradation pathway in cancer: therapeutic implications. Eur J Cancer 2004;40(15):2217–29.
[7] Mani A, Gelmann EP. The ubiquitin-proteasome pathway and its role in cancer. J Clin Oncol 2005;23(21):4776–89.
[8] Paramore A, Frantz S. Bortezomib. Nat Rev Drug Discov 2003;2(8):611–2.
[9] Adams J. The development of proteasome inhibitors as anticancer drugs. Cancer Cell 2004;5(5):417–21.
[10] Richardson PG, Sonneveld P, Schuster MW, Irwin D, Stadtmauer EA, Facon T, et al. Bortezomib or high-dose dexamethasone for relapsed multiple myeloma. N Engl J Med 2005;352(24):2487–98.
[11] Song L, Rape M. Reverse the curse – the role of deubiquitination in cell cycle control. Curr Opin Cell Biol 2008;20(2):156–63.
[12] Guterman A, Glickman MH. Deubiquitinating enzymes are IN/(trinsic to proteasome function). Curr Protein Pept Sci 2004;5(3):201–11.
[13] Grabbe C, Husnjak K, Dikic I. The spatial and temporal organization of ubiquitin networks. Nat Rev Mol Cell Biol 2011;12(5):295–307.
[14] Huang TT, D'Andrea AD. Regulation of DNA repair by ubiquitylation. Nat Rev Mol Cell Biol 2006;7(5):323–34.
[15] Messick TE, Greenberg RA. The ubiquitin landscape at DNA double-strand breaks. J Cell Biol 2009;187(3):319–26.
[16] Sacco JJ, Coulson JM, Clague MJ, Urbe S. Emerging roles of deubiquitinases in cancer-associated pathways. IUBMB Life 2010;62(2):140–57.
[17] Singhal S, Taylor MC, Baker RT. Deubiquitylating enzymes and disease. BMC Biochem 2008;9(Suppl. 1):S3.
[18] Todi SV, Paulson HL. Balancing act: deubiquitinating enzymes in the nervous system. Trends Neurosci 2011;34(7):370–82.
[19] Hussain S, Zhang Y, Galardy PJ. DUBs and cancer: the role of deubiquitinating enzymes as oncogenes, non-oncogenes and tumor suppressors. Cell Cycle 2009;8(11):1688–97.
[20] Komander D, Clague MJ, Urbe S. Breaking the chains: structure and function of the deubiquitinases. Nat Rev Mol Cell Biol 2009;10(8):550–63.
[21] Lee MJ, Lee BH, Hanna J, King RW, Finley D. Trimming of ubiquitin chains by proteasome-associated deubiquitinating enzymes. Mol Cell Proteomics 2011;10(5):R110.003871.
[22] Verma R, Aravind L, Oania R, McDonald WH, Yates 3rd JR, Koonin EV, et al. Role of Rpn11 metalloprotease in deubiquitination and degradation by the 26S proteasome. Science 2002;298(5593):611–5.
[23] Yao T, Song L, Xu W, DeMartino GN, Florens L, Swanson SK, et al. Proteasome recruitment and activation of the Uch37 deubiquitinating enzyme by Adrm1. Nat Cell Biol 2006;8(9):994–1002.

[24] Fraile JM, Quesada V, Rodriguez D, Freije JM, Lopez-Otin C. Deubiquitinases in cancer: new functions and therapeutic options. Oncogene 2012;31(19):2373–88.

[25] D'Arcy P, Brnjic S, Olofsson MH, Fryknas M, Lindsten K, De Cesare M, et al. Inhibition of proteasome deubiquitinating activity as a new cancer therapy. Nat Med 2011;17 (12):1636–40.

[26] Daviet L, Colland F. Targeting ubiquitin specific proteases for drug discovery. Biochimie 2008;90(2):270–83.

[27] Liu N, Liu C, Li X, Liao S, Song W, Yang C, et al. A novel proteasome inhibitor suppresses tumor growth via targeting both 19S proteasome deubiquitinases and 20S proteolytic peptidases. Sci Rep 2014;4:5240.

[28] Milacic V, Chen D, Giovagnini L, Diez A, Fregona D, Dou QP. Pyrrolidine dithiocarbamate-zinc(II) and -copper(II) complexes induce apoptosis in tumor cells by inhibiting the proteasomal activity. Toxicol Appl Pharmacol 2008;231(1): 24–33.

[29] Verani CN. Metal complexes as inhibitors of the 26S proteasome in tumor cells. J Inorg Biochem 2012;106(1):59–67.

[30] Zhao C, Chen X, Yang C, Zang D, Lan X, Liao S, et al. Repurposing an antidandruff agent to treating cancer: zinc pyrithione inhibits tumor growth via targeting proteasome-associated deubiquitinases. Oncotarget 2017;8(8):13942–56.

[31] Zhao C, Chen X, Zang D, Lan X, Liao S, Yang C, et al. A novel nickel complex works as a proteasomal deubiquitinase inhibitor for cancer therapy. Oncogene 2016;35(45): 5916–27.

[32] Li X, Liu S, Huang H, Liu N, Zhao C, Liao S, et al. Gambogic acid is a tissue-specific proteasome inhibitor in vitro and in vivo. Cell Rep 2013;3(1):211–22.

[33] Florea AM, Busselberg D. Cisplatin as an anti-tumor drug: cellular mechanisms of activity, drug resistance and induced side effects. Cancers (Basel) 2011;3(1):1351–71.

[34] Liu N, Li X, Huang H, Zhao C, Liao S, Yang C, et al. Clinically used antirheumatic agent auranofin is a proteasomal deubiquitinase inhibitor and inhibits tumor growth. Oncotarget 2014;5(14):5453–71.

[35] Bence NF, Sampat RM, Kopito RR. Impairment of the ubiquitin-proteasome system by protein aggregation. Science 2001;292(5521):1552–5.

[36] Liu J, Chen Q, Huang W, Horak KM, Zheng H, Mestril R, et al. Impairment of the ubiquitin-proteasome system in desminopathy mouse hearts. FASEB J 2006;20(2): 362–4.

[37] Chen X, Shi X, Zhao C, Li X, Lan X, Liu S, et al. Anti-rheumatic agent auranofin induced apoptosis in chronic myeloid leukemia cells resistant to imatinib through both Bcr/Abl-dependent and -independent mechanisms. Oncotarget 2014;5(19): 9118–32.

[38] Fiskus W, Saba N, Shen M, Ghias M, Liu J, Gupta SD, et al. Auranofin induces lethal oxidative and endoplasmic reticulum stress and exerts potent preclinical activity against chronic lymphocytic leukemia. Cancer Res 2014;74(9):2520–32.

[39] Yerushalmi R, Woods R, Ravdin PM, Hayes MM, Gelmon KA. Ki67 in breast cancer: prognostic and predictive potential. Lancet Oncol 2010;11(2):174–83.

[40] Tian Z, D'Arcy P, Wang X, Ray A, Tai YT, Hu Y, et al. A novel small molecule inhibitor of deubiquitylating enzyme USP14 and UCHL5 induces apoptosis in multiple myeloma and overcomes bortezomib resistance. Blood 2014;123(5):706–16.

[41] Chen D, Cui QC, Yang H, Barrea RA, Sarkar FH, Sheng S, et al. Clioquinol, a therapeutic agent for Alzheimer's disease, has proteasome-inhibitory, androgen receptor-suppressing, apoptosis-inducing, and antitumor activities in human prostate cancer cells and xenografts. Cancer Res 2007;67(4):1636–44.

[42] Chen D, Cui QC, Yang H, Dou QP. Disulfiram, a clinically used anti-alcoholism drug and copper-binding agent, induces apoptotic cell death in breast cancer cultures and xenografts via inhibition of the proteasome activity. Cancer Res 2006;66(21): 10425–33.

[43] Chen X, Yang Q, Xiao L, Tang D, Dou QP, Liu J. Metal-based proteasomal deubiquitinase inhibitors as potential anticancer agents. Cancer Metastasis Rev 2017;36(4):655–68.

[44] Cvek B, Milacic V, Taraba J, Dou QP. Ni(II), Cu(II), and Zn(II) diethyldithiocarbamate complexes show various activities against the proteasome in breast cancer cells. J Med Chem 2008;51(20):6256–8.

[45] Tomco D, Schmitt S, Ksebati B, Heeg MJ, Dou QP, Verani CN. Effects of tethered ligands and of metal oxidation state on the interactions of cobalt complexes with the 26S proteasome. J Inorg Biochem 2011;105(12):1759–66.

[46] Zhang X, Frezza M, Milacic V, Ronconi L, Fan Y, Bi C, et al. Inhibition of tumor proteasome activity by gold-dithiocarbamato complexes via both redox-dependent and -independent processes. J Cell Biochem 2010;109(1):162–72.

[47] Mukhopadhyay D, Riezman H. Proteasome-independent functions of ubiquitin in endocytosis and signaling. Science 2007;315(5809):201–5.

[48] Lee BH, Lee MJ, Park S, Oh DC, Elsasser S, Chen PC, et al. Enhancement of proteasome activity by a small-molecule inhibitor of USP14. Nature 2010;467(7312):179–84.

[49] Shah SA, Potter MW, McDade TP, Ricciardi R, Perugini RA, Elliott PJ, et al. 26S proteasome inhibition induces apoptosis and limits growth of human pancreatic cancer. J Cell Biochem 2001;82(1):110–22.

[50] Maertens GN, El Messaoudi-Aubert S, Elderkin S, Hiom K, Peters G. Ubiquitin-specific proteases 7 and 11 modulate Polycomb regulation of the INK4a tumour suppressor. EMBO J 2010;29(15):2553–65.

[51] Eichhorn PJ, Rodon L, Gonzalez-Junca A, Dirac A, Gili M, Martinez-Saez E, et al. USP15 stabilizes TGF-beta receptor I and promotes oncogenesis through the activation of TGF-beta signaling in glioblastoma. Nat Med 2012;18(3):429–35.

[52] Li J, Tan Q, Yan M, Liu L, Lin H, Zhao F, et al. miRNA-200c inhibits invasion and metastasis of human non-small cell lung cancer by directly targeting ubiquitin specific peptidase 25. Mol Cancer 2014;13:166.

[53] Lin Z, Yang H, Tan C, Li J, Liu Z, Quan Q, et al. USP10 antagonizes c-Myc transcriptional activation through SIRT6 stabilization to suppress tumor formation. Cell Rep 2013;5(6):1639–49.

[54] Yuan J, Luo K, Zhang L, Cheville JC, Lou Z. USP10 regulates p53 localization and stability by deubiquitinating p53. Cell 2010;140(3):384–96.

[55] Coughlin K, Anchoori R, Iizuka Y, Meints J, MacNeill L, Vogel RI, et al. Small-molecule RA-9 inhibits proteasome-associated DUBs and ovarian cancer in vitro and in vivo via exacerbating unfolded protein responses. Clin Cancer Res 2014;20(12):3174–86.

[56] Kapuria V, Peterson LF, Fang D, Bornmann WG, Talpaz M, Donato NJ. Deubiquitinase inhibition by small-molecule WP1130 triggers aggresome formation and tumor cell apoptosis. Cancer Res 2010;70(22):9265–76.

[57] Wang X, D'Arcy P, Caulfield TR, Paulus A, Chitta K, Mohanty C, et al. Synthesis and evaluation of derivatives of the proteasome deubiquitinase inhibitor b-AP15. Chem Biol Drug Des 2015;86(5):1036–48.

[58] Zhou B, Zuo Y, Li B, Wang H, Liu H, Wang X, et al. Deubiquitinase inhibition of 19S regulatory particles by 4-arylidene curcumin analog AC17 causes NF-kappaB inhibition and p53 reactivation in human lung cancer cells. Mol Cancer Ther 2013;12(8): 1381–92.